Submitted to J. Appl. Phys. on 10.05.2002

Superconducting trapped-field magnets: Temperature and field distributions during pulsed field activation

S. Bræck,[1] D. V. Shantsev,[1,2] T. H. Johansen,[1] and Y. M. Galperin[1,2]

[1] *Department of Physics, University of Oslo, PO Box 1048 Blindern, 0316 Oslo, Norway*
[2] *A. F. Ioffe Physico-Technical Institute of Russian Academy of Sciences, 194021 St. Petersburg, Russia*

We calculate the temperature and magnetic field distributions in a bulk superconductor during the process of pulsed-field magnetic activation. The calculations are based on the heat diffusion equation with account of the heat produced by flux motion, and the critical state model with temperature dependent critical current density. For a given activation time the total amount of trapped flux Φ is maximum for an optimal value $B_{\rm opt}$ of the maximal applied field. We analyze how $B_{\rm opt}$ and Φ depend on the material parameters and the field ramp rate.

I. INTRODUCTION

The recent progress in fabrication of large sized high-temperature superconductors with high critical current density makes them extremely promising for use as permanent magnets. Trapped fields exceeding 12 T have already been reported for a $YBa_2Cu_3O_{7-\delta}$ magnet at 22 K.[1] To magnetically activate the superconductor one most often uses a pulsed field magnetization (PFM). Whereas the PFM activation method is the most convenient from practical point of view, even higher fields have been trapped by quasi-static field ramping.[2,3,4,5] This shortcoming of PFM cannot be overcome by simply increasing the maximal applied field B_M. In fact, it is found experimentally that the trapped flux reaches maximum at some optimal value $B_M = B_{\rm opt}$, and decreases for larger B_M.[2,3,4,5,6,7,8] This behavior is believed to result from heating produced by flux motion, which leads to strong temperature rise in superconductor during the activation process. There have already been suggested practical ways to improve the situation, in particular, by applying multiple field pulses.[4,6,9] Even better results can be expected if the development is accompanied by a modeling of how the heat actually dissipates and redistributes in a superconductor during the PFM. Surprisingly, almost no efforts have been done in this direction, and this lack of insight motivates the present work.

Our analysis is based on the heat diffusion equation, taking into account the time and position dependent heat dissipation due to flux motion. As a result, the temperature and magnetic field distributions in the superconductor during all the stages of the PFM process are calculated. We determine the optimal applied field $B_{\rm opt}$ corresponding to the maximum trapped flux $\Phi(B_{\rm opt})$ and analyze how $B_{\rm opt}$ and $\Phi(B_{\rm opt})$ depend on the parameters of superconductor.

II. EQUATIONS AND BASIC APPROACH

The distributions of magnetic field, $\mathbf{B}$, electric field $\mathbf{E}$ and current density $\mathbf{j}$ inside a sample are determined by the Maxwell equations

$$\nabla \times \mathbf{B} = \mu_0 \mathbf{j}\,, \tag{1}$$

$$\nabla \times \mathbf{E} = -\partial \mathbf{B}/\partial t\,. \tag{2}$$

These equations should be supplemented by a relationship between $\mathbf{j}$ and the fields $\mathbf{E}$ and $\mathbf{B}$, which depends on the superconductor material, as well as on temperature T. When a superconductor is subjected to a non-stationary external magnetic field, $B_a(t)$, a heat per unit volume is produced with the rate

$$W = \mathbf{E}\cdot\mathbf{j}\,. \tag{3}$$

The heat release creates a temperature rise which is given by the thermal diffusion equation

$$C\,\partial T/\partial t - \kappa \nabla^2 T = W\,. \tag{4}$$

Here κ is the thermal conductivity, and C the heat capacity per volume.

For simplicity we will make calculations for a superconductor shaped as a slab, while we expect that all qualitative results are valid also for other geometries. The superconductor occupies space $|x| \le w$, and satisfies the boundary condition $T(|x| = w) = T_0$, which assumes ideal thermal contact with the surroundings at the temperature T_0. The solution for a uniform initial temperature can be expressed as

$$T(x,t) = T_0 + \int_{-w}^{w} dx' \int_0^t dt'\, G(x,t;x',t')\,\frac{W(x',t')}{C}, \tag{5}$$

where $G(x,t;x',t')$ is the Green's function due to a unit instantaneous plane source at x' at t'. The Green's function satisfying the boundary conditions $G(x = \pm w, t; t', x') = 0$ is given by[10]

$$G(x,t;x',t') = \frac{1}{w}\sum_{n=1}^{\infty}\left(\cos^2\frac{n\pi}{2}\sin\frac{n\pi x}{2w}\sin\frac{n\pi x'}{2w} + \sin^2\frac{n\pi}{2}\cos\frac{n\pi x}{2w}\cos\frac{n\pi x'}{2w}\right) e^{-\kappa n^2\pi^2(t-t')/4Cw^2}. \tag{6}$$

To calculate heat release rate $W(x,t)$ we use the critical state model, according to which the magnitude of the current density in flux-penetrated regions of a superconductor equals to some critical value, j_c. The critical current density depends in general on both the local field B and local temperature T, thus the magnetic field profile is determined by Eq. (1) with $|\mathbf{j}| = j_c(B,T)$. In order to obtain analytical results, we choose the Bean model, i. e. assume j_c to be B independent. To account for the T dependence of j_c the following iterative procedure is used. First, j_c is taken T-independent and the time evolution of the profiles $B(x,t)$ and $W(x,t)$ is calculated. The W is substituted in Eq. (5) to determine the temperature profile $T(x,t)$. It is then used to recalculate the $j_c[T(x,t)]$ which subsequently gives corrected magnetic field profiles according to Eq. (1). Fortunately, it turns out that even the 1st iteration gives correct results within very good accuracy for realistic parameters. This is demonstrated below by a self-consistent numerical solution of the above set of equations.

Let us consider a PFM where the external field is applied as a triangular pulse,

$$B_a(t) = R\,(t_M - |t - t_M|)\,, \tag{7}$$

where R is a constant ramp rate, i. e. the field increases to the maximum value B_M during $0 \le t \le t_M = B_M/R$, and then decreases to zero during $t_M < t \le 2t_M$. When the temperature dependence of the critical current is neglected the field profile is given by the conventional Bean model for a zero-field-cooled superconductor, i.e., when the external field *increases*, the magnetic flux occupies the region $x_0(t) \le |x| \le w$, where

$$x_0(t) = w - vt\,, \quad v = R/\mu_0 j_{c0}\,, \quad j_{c0} \equiv j_c(T_0)\,. \tag{8}$$

The heat release in the penetrated region is obtained from Eqs. (2) and (3):

$$W(x,t) = [|x| - x_0(t)]\,Rj_{c0} \tag{9}$$

while $W(x,t) = 0$ at $|x| < x_0(t)$. After the sample becomes fully penetrated, i. e. at $t \ge w/v$, one has

$$W(x,t) = |x| R j_{c0}\,. \tag{10}$$

Similarly, for *decreasing* applied field we obtain

$$W(x,t) = [|x| - x_1(t)]\,Rj_{c0}\,, \quad x_1(t) \le |x| \le w\,, \tag{11}$$

where

$$x_1(t) = w - v(t - t_M)/2 \tag{12}$$

is the position of maximum flux density. In the region $|x| < x_1(t)$ there is no flux motion, and therefore no heat release. For $t > t_M + 2w/v$ the field is decreasing throughout the sample, and the dissipation is again given by Eq. (10). From this set of $W(x,t)$ one finds the temperature distributions $T(x,t)$ at all stages of the process. The expressions are listed in the Appendix. Finally, we determine the refined $B(x,t)$) by assuming a linear T dependence of the critical current,

$$j_c(x,t) = j_{c0}\,\frac{T_c - T(x,t)}{T_c - T_0} \tag{13}$$

where T_c is the critical temperature.[11]

The present thermo-magnetic problem is characterized by only two dimensionless parameters. The first is the ratio of t_M to the thermal diffusion time Cl^2/κ,

$$\tau = t_M \kappa / Cl^2 = B_M \kappa / RCw^2\,. \tag{14}$$

If $\tau \ll 1$ the heat diffusion can be neglected, whereas for $\tau \gg 1$ the heat escapes the sample so fast that the temperature increase is negligible. The second parameter is

$$\alpha = \frac{B_p}{B_{fj}} = \left(\frac{\mu_0 w^2 j_{c0}}{2C}\,\frac{\partial j_c}{\partial T}\right)^{1/2}\,. \tag{15}$$

Here $B_p = \mu_0 j_{c0} w$ is the full penetration field, and B_{fj} is the threshold field for a flux jump.[12,13] Consideration of flux jumps – macroscopic flux avalanches accompanied by pronounced heating – is beyond the scope of the present study. In practice, one wants to avoid flux jumps, which ruin the magnetization process, and can even damage the material. Therefore we limit ourselves to the parameter range where $\alpha < 1$, and where the above iteration procedure is applicable.

III. RESULTS AND DISCUSSION

We present results of the calculations assuming a sample of size $2w = 1$ cm and characterized by $j_{c0} = 4.4 \cdot 10^8$ A/m^2 (giving $B_p \approx 2.8$ T), $C = 0.88 \times 10^6$ J/m^{3}K, and $\kappa = 6$ J/msK, all of which are typical values for $YBa_2Cu_3O_{7-\delta}$ crystal with $T_c = 92$ K at $T_0 = 77$ K. From Eq. (13) one finds that the above set of parameters corresponds to $\alpha = 0.48 < 1$.

Shown in Figs. 1 and 2 are the temperature and field distributions after completed PFM, i.e., in the remanent state at $t = 2t_M$. The figures display the result for the cases $B_M = 2B_p$ and $B_M = 1.6B_p$, and the profiles are plotted for four different ramp rates of the applied field, corresponding to τ ranging from 1 to 0.001. At high rates the temperature profiles have pronounced maxima near the sample surface. The reason is obvious – near the surface the flux motion is most intense and the heat release is maximal, see Eqs. (9)-(11). For a high ramp rate ($\tau \ll 1$), the heat remains mostly in the regions where it was released. If the rate is low ($\tau \gtrsim 1$) the heat has time to diffuse both to the center and the surface. As a result, $T(x,t)$ becomes more uniform, but on the average the temperature rise is smaller than for high rates.

As seen from the lower panels the temperature rise strongly affects the profiles of the remanent field. Increased temperatures give a lower critical current, and hence, less steep slopes $|\partial B/\partial x| = \mu_0 j_c(T)$. For the highest ramp rate the profiles are also most non-linear, and

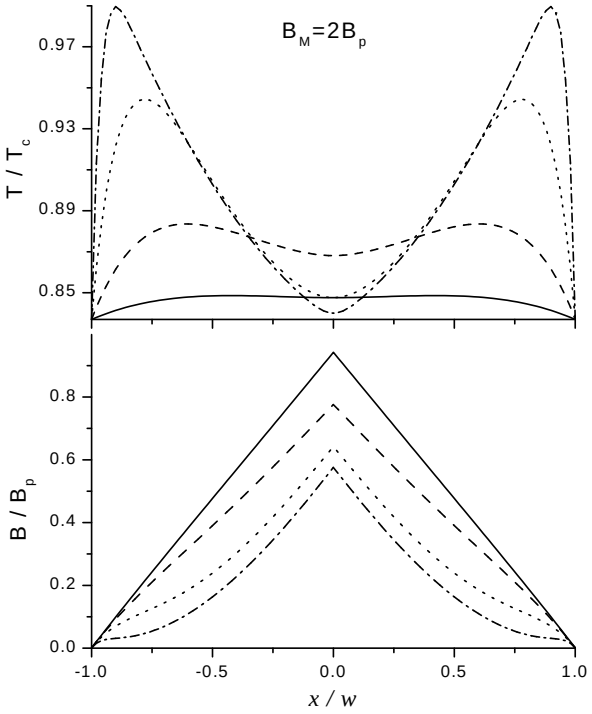

FIG. 1: Temperature and flux density profiles in the remanent state after application of magnetic field $B_M = 2B_p$. Four curves are calculated for different durations of the field pulse: $2t_M = 7.3$ s (solid), 0.73 s (dashed), 73 ms (dotted) and 7.3 ms (dash-dotted), which correspond to $\tau = 1$, 0.1, 0.01 and 0.001, respectively.

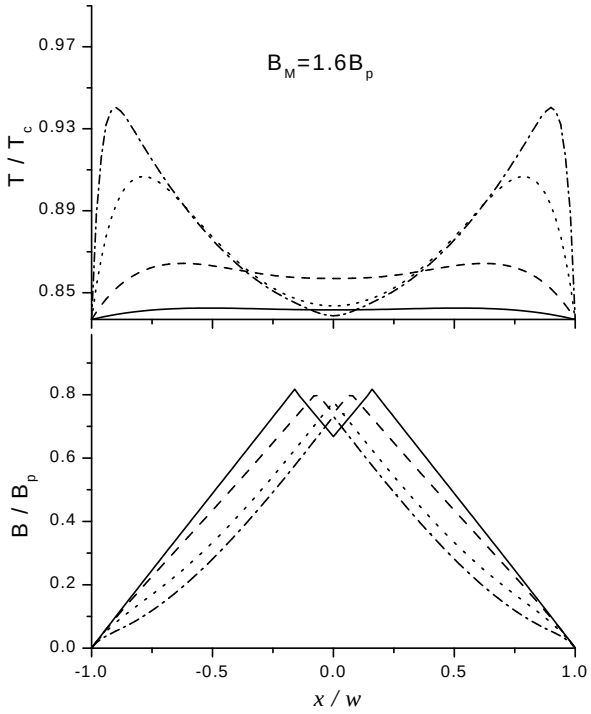

FIG. 2: The same curves as in Fig. 1 but for the maximum applied field $B_M = 1.6B_p$.

the total amount of trapped flux is lowest. Hence, we reproduce the expected result that very low ramp rates give maximum trapped flux.

In practice, the duration of the field pulse is limited. The key point is then to choose the optimum applied field B_M so that in the remanent state the trapped flux becomes maximum. If B_M is too small the flux penetration is also small, whereas too large B_M gives an excessive heating and little flux becomes trapped by the sample. This is illustrated in Fig. 3, where the total amount of trapped flux $\Phi = \int B(x)dx$ per unit length of the slab is plotted as a function of B_M. The solid curves show the conventional Bean-model result,

$$\begin{aligned} \Phi &= wB_M^2/(2B_p), \quad B_M \le B_p, \\ &= w\left[2B_M - B_p - B_M^2/(2B_p)\right], \quad B_p \le B_M \le 2B_p, \\ &= wB_p, \quad B_M \ge 2B_p, \end{aligned} \tag{16}$$

obtained for a slab superconductor assuming linear field profiles. This result is applicable when the heating is negligible, i.e., for very low ramp rates or large C or κ, i.e., when $\tau \to \infty$ or $\alpha \to 0$. The presence of heating leads to reduction of the trapped flux, and a peak in the $\Phi(B_M)$ curve appears at some B_M between B_p and $2B_p$. The two panels of Fig. 3 allow us to trace the effect of changing the parameters τ and α. Plotted as symbols in Fig. 3 are the exact results obtained by numerical simulations, whereas the lines represent the analytical solution. For the most important range of B_M where Φ has the peak, the agreement is excellent, and only a slight deviation appears for large B_M. We conclude therefore that the model given by Eqs.(5), (6), (9)-(11) allows to determine the B_M producing the maximum trapped flux.

Let us consider 3 characteristic points, A, B and C on the $\Phi(B_M)$ where the peak is most pronounced, and analyze the corresponding B and T distributions. These remanent profiles are shown in Fig. 4. For small B_M (A) too little flux penetrated the superconductor, and the $B(x)$ profile has a large dip in the center region. For large B_M (C), the $B(x)$ profile has the "right" triangular shape, however, its slopes are not maximally steep due to heating. In the state of maximum trapped flux (B) the small dip in the center is compensated by having relatively large slopes in the overall peak. Interestingly, we find that the optimum case always has a small minimum in the flux density at the center of the superconductor.

If the maximum applied field is very large, the heat is most of the time released uniformly throughout the superconductor. Meanwhile, the heat is removed only through the surface which is maintained at a fixed temperature. As a result, the remanent $T(x, 2t_M)$ has a broad maximum in the center, and the trapped $B(x, 2t_M)$ acquire a specific "bell" shape. This is illustrated in Fig. 5 for the case $B_M = 6B_p$.

It is also interesting to analyze the evolution of the

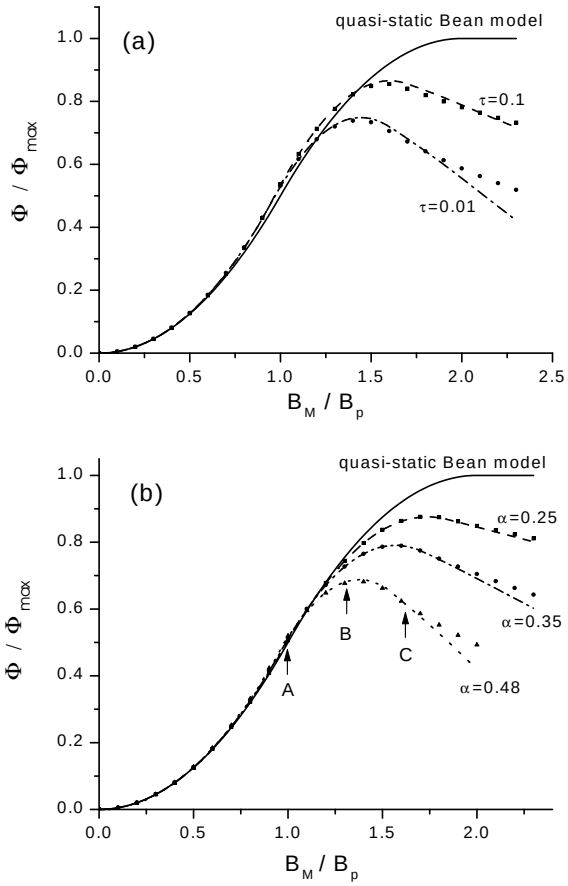

FIG. 3: Trapped remanent flux after a magnetization process for different maximum applied fields B_M. (a) Curves for $\alpha = 0.48$ and different τ, i. e., for different rates. (b) Curves for $\tau = 0.001$ and different α, i. e., for different heat capacities. The solid curve is the same for both plots and shows the Bean-model result without any heating effects. Symbols show results of numerical calculations which reproduce well our analytical curves except for very large B_M.

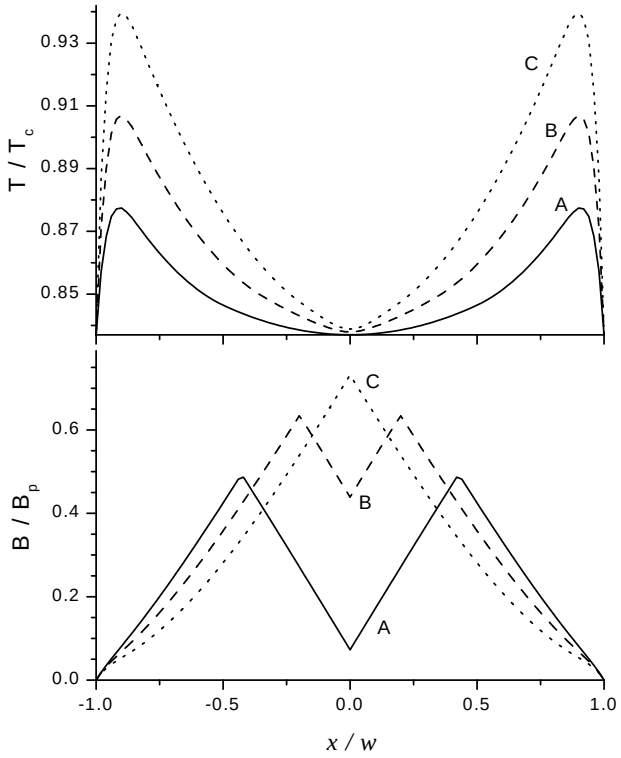

FIG. 4: Temperature and flux density profiles in the remanent state after application of the maximum field $B_M = B_p$ (A), $B_M = 1.3B_p$ (B), and $B_M = 1.6B_p$ (C). The profiles correspond to the marked points (A,B,C) on the lowest curve of Fig. 3(b). The profile (B) corresponds to the maximum trapped flux.

temperature and flux density during the whole magnetization process. A time sequence of curves showing this is plotted in Fig. 6, and corresponds to the intermediate stages leading to the remanent state seen in Fig. 1 for $\tau = 0.001$. One can see that the temperature growth starts slowly and then accelerates. When the applied field reaches maximum (at $t = t_M$), the T profile has already acquired its characteristic shape and changes little during the subsequent field decrease. The evolution of the B profile looks similar to the standard Bean-model behavior. The full penetration is reached approximately at $B_a = B_p$ (at $t = t_M/2$), and then the $B(x,t)$ shifts upward almost uniformly until the field starts to decrease and flux exits from the surface. The flux front position (seen as a ridge in the 3D plot) is shifting towards the center, and in the final remanent state the B profile acquires its triangular shape.

Our approach, used so far for a constant ramp rate of the field, is easily generalized to having different sweep rates on the ascending and descending field branch. It turns out that for a given magnetization time it is somewhat beneficial to have a faster field increase followed by a slower decrease to zero. In particular, for the extreme case of an instantaneous field increase and a descent lasting 8 ms we find that one traps 8% more flux than for the symmetric 4+4 ms field pulse (for the parameters used in the paper). The physical reason for this is the following. When a larger amount of heat is dissipated in the beginning of the PFM, the heat has more time to flow out of the sample. As a result, the temperature in the remanent state becomes slightly lower, which results in a larger trapped flux. We omit to show detailed profiles, since these graphs are very similar to the ones already presented in this paper.

The critical state model used in our analysis neglects the viscous force acting on flux lines. This force can be an important ingredient that determines the $B(x,t)$ distributions during very fast PFM.[7] We stress, however, that the heating takes place independent of whether the flux motion is viscous or not. Our results clearly demonstrate that the heating produced within the critical-state approach is sufficient to account for the suppression of the trapped flux during the PFM process.

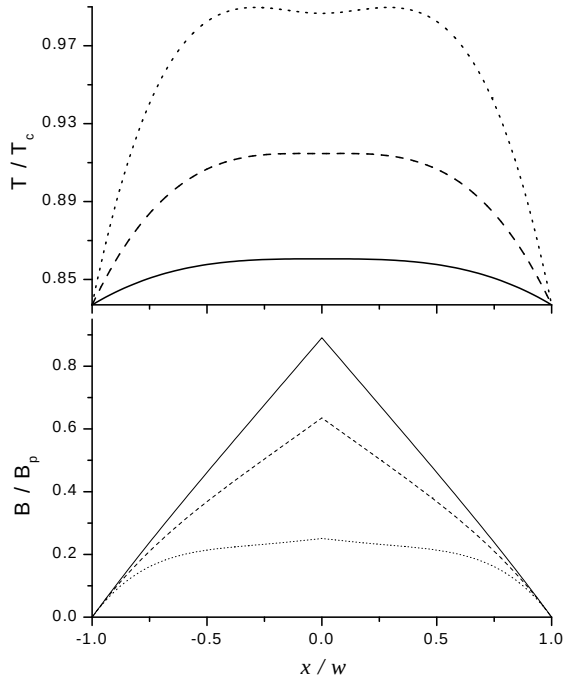

FIG. 5: Temperature and flux density profiles in the remanent state after applying magnetic field $B_M = 6B_p$. The curves are obtained for the field-pulse duration: 23.2 s (solid), 6.3 s (dashed), and 2.3 s (dotted), which correspond to τ=3.2, 0.9 and 0.32, respectively.

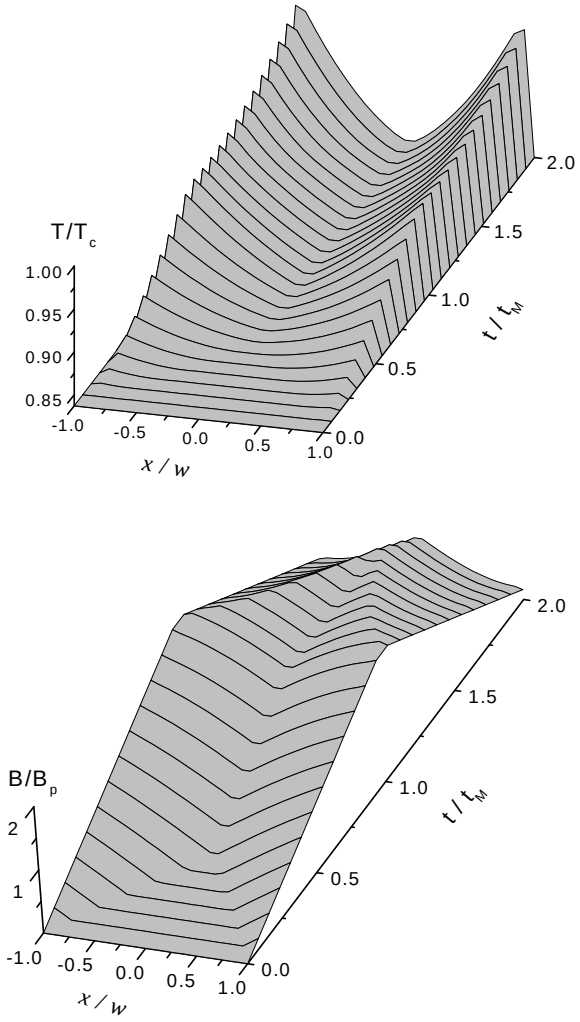

FIG. 6: Time evolution of temperature and flux density distrbutions during the full magnetization process for the maximal field $B_M = 2B_p$, and duration 7.3 ms (τ=0.001).

IV. CONCLUSION

The temperature and field distributions in a bulk superconductor during a PFM process are calculated analytically within the critical state model and with account of heating due to flux motion. The remanent trapped flux Φ is smaller for a larger PFM rate, and for smaller heat capacity. For a given duration of the activation pulse the Φ reaches maximum for some optimal maximum field, which is always smaller than twice the penetration field. Suprizingly, the remanent flux distribution for optimal field is not monotonous, but the overall peak has a small dip in the center. The strongest temperature rise is usually found close to the surface. The trapped flux can be enhanced without changing the total PFM time if the field ascent is made faster than the descent to zero.

APPENDIX A

Here we list analytical expressions for the temperature distribution for different stages of the magnetization process. They are obtained by substituting the heat release rate given by Eqs.(9)-(11) and the Green function (6) into Eq. (5). The expressions are given for a general case of having different field ramp rates R_A and R_D on the ascending and descending branch, respectively. The following notations are used: $a = \pi^2\kappa/4Cw^2$ (inverse thermal diffusion time), $b = \pi/(2aB_p)$, and t_M is the time when the applied field reaches maximum, $t_M = B_M/R_A$. The temperature distribution during the magnetization process is given by

$$T(x,t) = T_0 + \frac{32 j_{c0} w^3 R_A}{\pi^4 \kappa} \sum_{n=1}^{\infty} S_n(t) \ \sin\frac{n\pi}{2} \cos\frac{n\pi x}{2w} \tag{A1}$$

The dimensionless coefficient S_n are given by one of the expressions below, and Tab. 1 explains which expression should be used for every particular case. It is convenient to define the following functions corresponding to incom-

$B_M \le B_p$	$t \le t_M$	(A4)
	$t_M < t \le t_M + B_M/R_D$	(A5)
$B_p \le B_M \le 2B_p$	$t \le B_p/R_A$	(A4)
	$B_p/R_A < t \le t_M$	(A6)
	$t_M < t \le t_M + B_M/R_D$	(A7)
$B_M \ge 2B_p$	$t \le B_p/R_A$	(A4)
	$B_p/R_A < t \le t_M$	(A6)
	$t_M < t \le t_M + 2B_p/R_D$	(A7)
	$t_M + 2B_p/R_D < t \le t_M + B_M/R_D$	(A8)

TABLE I: The last column shows which formula for coefficients S_n in Eq. (A1) should be used for given B_M and t.

plete and complete penetration processes:

$$S_n^{\rm inc}(t,R) \equiv \frac{(an^2t + e^{-an^2t} - 1)bR}{n^5} + \frac{\left[\cos(abRnt) - e^{-an^2t}\right] bR/n - \sin(abRnt)}{n^2\left[n^2 + (bR)^2\right]}\,, \quad \text{(A2)}$$

$$S_n^{\rm com}(t,R) = \frac{e^{-an^2(t-B_p/R)}}{n^3}\left\{\frac{\pi}{2} - \frac{bR}{n^2} + \frac{(bR)^3\ e^{-an^2B_p/R} - n^3\sin\frac{n\pi}{2}}{n^2\left[n^2+(bR)^2\right]} + \left(\frac{\pi}{2}\sin\frac{n\pi}{2} - \frac{1}{n}\right)\sin\frac{n\pi}{2}\left(e^{an^2(t-B_p/R)} - 1\right)\right\}, \quad \text{(A3)}$$

Then,

$$S_n = S_n^{\rm inc}(t,R_A)\,, \quad \text{(A4)}$$

$$S_n = e^{-an^2(t-t_M)}S_n^{\rm inc}(t_M,R_A) + \frac{R_D}{R_A}\,S_n^{\rm inc}(t-t_M,R_D/2)\,, \quad \text{(A5)}$$

$$S_n = S_n^{\rm com}(t,R_A)\,, \quad \text{(A6)}$$

$$S_n = e^{-an^2(t-t_M)}S_n^{\rm com}(t_M,R_A) + \frac{R_D}{R_A}\,S_n^{\rm inc}(t-t_M,R_D/2)\,. \quad \text{(A7)}$$

$$S_n = e^{-an^2(t-t_M)}S_n^{\rm com}(t_M,R_A) + \frac{R_D}{R_A}\,S_n^{\rm com}(t-t_M,R_D/2) \quad \text{(A8)}$$

* Email: t.h.johansen@fys.uio.no

[1] S. Gruss, G. Fuchs, G. Krabbes, P. Verges, G. Stöver, K.-H. Müller, J. Fink, and L. Schultz, Appl. Phys. Lett. **79** (2001) 3131.

[2] U. Mizutani, H. Ikuta, T. Hosokawa, H. Ishihara, K. Tazoe, T. Oka, Y. Itoh, Y. Yanagi and M. Yoshikawa, Supercond. Sci. Technol. **13** (2000) 836.

[3] H. Ikuta, H. Ishihara, T. Hosokawa, Y. Yanagi, Y. Itoh, M. Yoshikawa, T. Oka and U. Mizutani, Supercond. Sci. Technol. **13** (2000) 846.

[4] H. Ikuta, Y. Yanagi, H. Ishihara, M. Yoshikawa, Y. Itoh, T. Oka and U. Mizutani, Physica C **357** (2001) 837.

[5] A. B. Surzhenko, S. Schauroth, D. Litzkendorf, M. Zeisberger, T. Habisreuther and W. Gawalek, Supercond. Sci. Technol. **14** (2001) 770.

[6] M. Sander, U. Sutter, R. Koch and M. Kläser, Supercond. Sci. Technol. **13** (2000) 841.

[7] Y. Itoh and U. Mizutani, Jpn. J. Appl. Phys. **35** (1996) 2114.

[8] Y. Itoh, Y. Yanagi, M. Yoshikawa, T. Oka, Y. Yamada, and U. Mizutani, Jpn. J. Appl. Phys. **35** (1996) L1173.

[9] M. Sander, U. Sutter, M. Adam and M. Klaser, Supercond. Sci. Technol. **15** (2002) 748.

[10] H. S. Carslaw and J. C. Jaeger, *Conduction of Heat in Solids* (Clarendon Press, Oxford, 1959).

[11] The determination of $B(x,t)$ is straighforward when the magnetic field either increases or decreases throughout the sample. Otherwise, there is a kink in the field profile. In the zeroth approximation, the kink position is given by Eqs. (8) and (12) for $x_0(t)$ or $x_1(t)$, for increasing/decreasing field, respectively. With account of the position-dependent temperature, these quantities can be obtained from the equations

$$\mu_0\int_{x_0(t)}^{w} j_c[T(x,t)]\,dx = B_a(t)\,,$$
$$\mu_0\int_{x_1(t)}^{w} j_c[T(x,t)]\,dx = B_a(t) - B[x_1(t),t_M]\,.$$

[12] S. L. Wipf, Phys. Rev. **161**, (1967) 404.

[13] S. L. Wipf, Cryogenics **31**, (1991) 936.